Application of electrochemical impedance spectroscopy for fuel cell characterization: polymer electrolyte fuel cell (pefc) and oxygen reduction reaction in alkaline solution

N. Wagner

German Aerospace Center, Institute for Technical Thermodynamics, Pfaffenwaldring 38-40, D-70569 Stuttgart, Germany

One of the most common method used to characterize the electrochemical performance of fuel cells is recording of current/voltage U(i) curves. Separation of electrochemical and ohmic contributions to the U(i) characteristics requires additional experimental techniques like Electrochemical Impedance Spectroscopy (EIS) or current interrupt method (CI). The application of EIS is an in-situ approach to determine parameters which have proved to be indispensable for the characterization and development of all types of fuel cell electrodes and electrolyte electrode assemblies [1]. In addition to EIS semi-empirical approaches based on simplified mathematical models can be used to fit experimental U(i) curves [2].

By varying the operating conditions of the fuel cell and by simulation of the measured EIS with an appropriate equivalent circuit, it is possible to split the cell impedance into electrode impedances and electrolyte resistance. Integration in the current density domain of the individual impedance elements enables the calculation of the individual overpotentials in the fuel cell (PEFC) and the assignment of voltage loss to the different processes. In case of using a three electrode cell configuration with a reference electrode one can determine directly the corresponding overvoltage. For the evaluation of the measured impedance spectra the porous electrode model of Göhr [3] was used. This porous electrode model includes different impedance contributions like impedance of the interface porous layer/pore, interface porous layer/electrolyte, interface porous layer/bulk, impedance of the porous layer and impedance of the pores filled by electrolyte.

Keywords: Electrochemical Impedance Spectroscopy, Porous Electrode Models, PEFC, AFC, Oxygen Reduction Reaction, Gas Diffusion Electrode, Diffusion

INTRODUCTION

Fuel cells allow an environmentally friendly and highly efficiently conversion of chemical energy to electricity and heat. Therefore, they have a high potential to become important components of an energy-efficient and sustainable economy. The main challenges in the development of fuel cells are cost reduction and long-term durability. Whereas the cost can be significantly reduced by innovative mass production, the knowledge to enhance the life time sufficiently is presently not available.

Low temperature (T<90ºC) fuel cells like Polymer Electrolyte Fuel Cells (PEFC) and Alkaline Fuel Cells (AFC) are promising for pollution-free energy supplying different applications. Alkaline fuel cells are in some respects an interesting alternative to polymer electrolyte membrane fuel cells. In AFC no expensive platinum metal or noble metal alloys are necessary. Nickel (usually Raney-Nickel) can be used for the hydrogen oxidation reaction (catalyst in the anode) and on the cathode silver can be used as catalyst for the oxygen reduction reaction, because the alkaline electrochemical environment in AFC is less corrosive compared to acid fuel cell conditions. In addition, using liquid alkaline solution as electrolyte heat balance and water management is enhanced. However, normally an electrolyte cycle is needed to remove the product water from the cell, but the electrolyte cycle can also be used as a cooling cycle. A major disadvantage is that AFC are typically operated with pure gases, in particular oxygen instead of air.

The life time of fuel cells is a decisive factor for their commercialization. Therefore, the degradation of fuel cell components is under increased investigation and mainly focused on PEFC [4–10]. Although for alkaline fuel cells several studies of degradation processes exist [11–13], they are all focussed on the electrodes, because the electrolyte in AFCs can be easily exchanged. In the case of using the silver GDE in a complete alkaline fuel cell, the high solubility of silver can lead in certain

circumstances to a transfer of silver to the anode and a resulting metal deposition associated with a decrease of activity of the anode. Open circuit situations of the cell may lead to oxidation of silver. A known degradation mechanisms of both AFC and PEFC is carbon corrosion of the catalyst support on the cathode which is accelerated by higher temperatures and higher potentials (e.g. at OCV). Shut down and restarting procedures can lead to enhanced degradation too.

Even if the operation and the components of PEFC and AFC are significantly distinct, for the electrochemical characterization one can use the same measuring technique (EIS) and for the evaluation of the experimental data the same porous electrode model. This paper deals with EIS investigation of:

- Polymer Electrolyte Fuel Cell with a solid proton conducting polymer membrane as electrolyte and electrodes impregnated with electrolyte suspension before use
- Silver gas diffusion cathode during oxygen reduction reaction used in Alkaline Fuel Cells with liquid alkaline electrolyte.

EXPERIMENTAL

In this paper two different experimental set-ups are used. In the case of PEFC the cell impedance of the whole fuel cell consisting of anode, proton conducting membrane and cathode is determined during one measurement without using a reference electrode. In the case of AFC, given by the liquid electrolyte a three electrode cell (half-cell) configuration with a reference electrode is applicable, so that each electrode (anode or cathode) can be investigated separately.

Application of EIS for PEFC characterization

The investigated PEFC electrodes were commercial electrodes from EЇTEK (20% Pt/C, 0.4 mg/cm^2, thickness 200 μm) impregnated before use with 1 mg/cm^2 Nafion suspension, Aldrich Chemie and with Nafion® 117 as electrolyte. After pretreatment (activation) of the Nafion membrane with H_2O_2/H_2SO_4, electrodes and membrane have been hot pressed (1.6 MPa, increasing temperature up to 160ºC) for 10 minutes. The resistance of the proton exchange membrane shows a strong dependence on water content. The fuel cell was operated at 80ºC with the hydrogen feeds stream humidified by passage through a bubbling bottle at
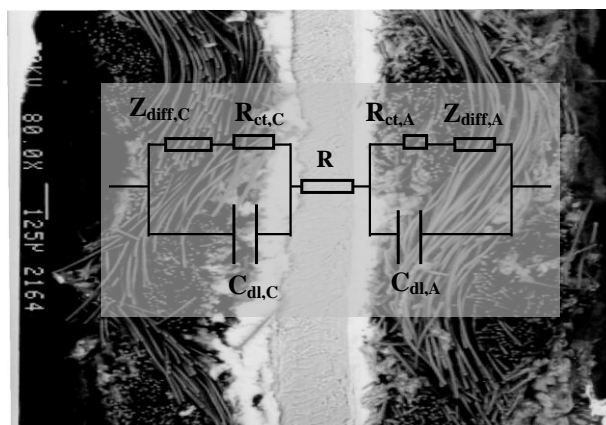
Fig. 1. Common equivalent circuit (EC) used for the simulation of fuel cells

a temperature of 90ºC. The oxygen was not humidified, it was only heated up to 30ºC before it entered the cell. Pure hydrogen and oxygen were used, both at 2.0 bar absolute. The hydrogen flow was „dead end" whereas the oxygen flow rate was adapted to twice the stoichiometric requirement at each current density. The geometric surface of the electrodes used in the PEFC is 23 cm^2.

The electrochemical characterization of the fuel cells was performed by electrochemical impedance measurements in the frequency range from 10 mHz to 4 MHz (IM6, Zahner-elektrik, Kronach, Germany). Measurements at currents up to 25 A have been carried out in combination with an external electronic load (Power potentiostat PP240 from Zahner-elektrik). Such high currents lead, however, to a limitation in the upper frequency range (<100 kHz), due to the low impedance of the fuel cell at frequencies higher than 10 kHz (at PEFC with 25 cm^2 active surface typically lower than 5ºmΩ) and to a mutual induction artefact [14].

Applying a three electrode cell with one reference electrode is complex for the investigation of electrochemical systems with solid electrolytes. Therefore, the anode and cathode transfer functions have been determined independently without a reference electrode using symmetric gas supply of hydrogen or oxygen on both electrodes of the fuel cell at open circuit potential (OCP). Thus, cathode and anode impedance can be determined directly with two independent experiments and appropriate equivalent circuits are derived to analyze the impedance response of the fuel cell at different current densities. Furthermore, by varying the electrode composition [15] and experimental conditions (temperature, gas composition and humidification) the measured cell impedance under load can be split up into anode impedance, cathode impedance and electrolyte resistance without using reference electrodes [16–17]. A general equivalent

circuit that can be used for the evaluation of measured spectra at fuel cells is shown in Fig.1. Under certain operating conditions (e.g. use of reference electrode) and in function of the fuel cell type one or more impedance elements from Fig. 1 can be omitted.

Results

Impedance spectra are presented as Bode plots, where the logarithm of the impedance magnitude and phase-shift are plotted vs. the logarithm of the frequency. To identify and separate the different diffusion processes, it is useful to represent the measured impedance spectra also as Nyquist diagram (imaginary part vs. real part of the impedance). In the Nyquist diagram one can observe the Nernst-impedance (finite diffusion) as an additional loop at the lowest part of the frequency range, the Warburg-impedance (infinite diffusion) as a straight line with a slope of 1 (real part = imaginary part). In the Bode diagram due to the logarithmical scale of the impedance the difference of the two kinds of diffusion can not be discerned so clearly.

EIS measured on the PEFC (H_2/O_2) in the potential range from OCV (1024 mV) to 600°mV (Fig.2) show in the Bode representation in the low frequency range of the spectra an exponential potential dependency of the impedance reaching a minimum at 600 mV (9 A). At cell voltages below 600 mV one can observe an increase of the cell impedance (e.g. spectra measured at 317 mV in Fig.1) and an additional phase-shift maximum at 50 mHz. The appearance and the nature of the new impedance contribution can be better seen from the Nyquist representation in Fig.3. From this increase of the cell impedance, one can deduce that at higher load of the cell an additional overvoltage occurs. From the shape of impedance spectra we can identify this additional overvoltage as a diffusion overvoltage. In this case it is a finite diffusion, corresponding to the „Nernst-impedance" as defined in equation (4) below, for details see [1].

Given the time constant of the mass transport, the impedance related to the diffusion is usually found at the lowest region of the frequency range. Therefore, the impedance has to be measured in a wide frequency range, down to 10 mHz or even lower.

In order to evaluate the measured impedance spectra, the reaction steps can be translated into an appropriate equivalent circuit (EC) which contains various impedance elements representing the involved reaction steps. Starting point is the general

EC shown in Fig. 1. For the evaluation of EIS shown in Fig. 2 and Fig. 3 one can use the EC shown inside Fig.4. In Fig.4 EIS spectra measured in the low cell voltage range (high current range) of PEFC are shown, whereas the points represent the measured data and the solid lines the simulated data after fitting the spectra with the corresponding EC.
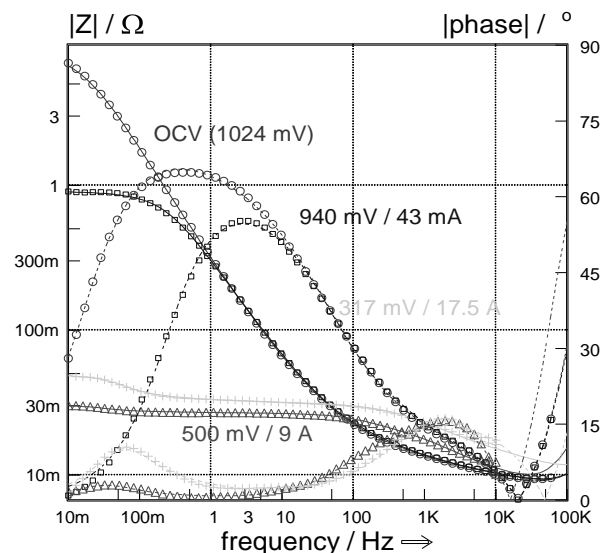

Fig. 2. Bode diagram of selected EIS measured on PEFC, 80°C, at 2 bar absolute, at different cell voltages (currents): (o) 1024 V, (□) 940 mV, (Δ) 500 mV and (+) 317 mV.
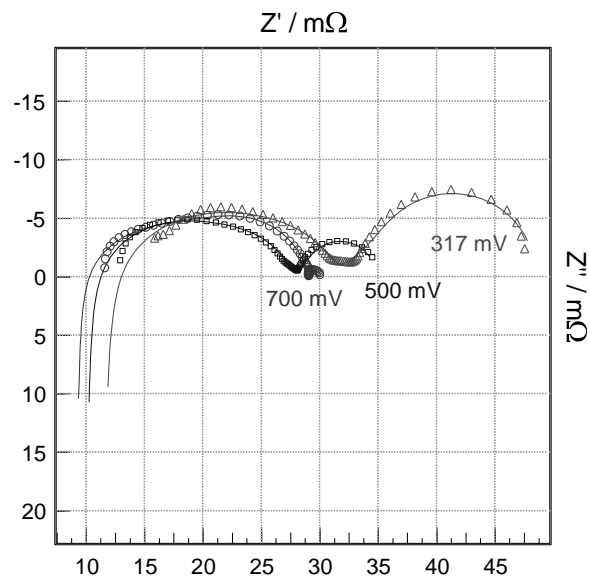
Fig. 3. Nyquist diagram of selected EIS measured on PEFC at low cell voltages, 80°C, at 2 bar absolute, at different cell voltages (currents): (o) 700 mV (5.4 A), (□) 500 mV (12.1 A) and (Δ) 317 mV (17.5 A).

The EC consist of a series resistance (electrolyte or membrane resistance R_{el}) and 3 parallel R/C terms which three different potential depending time constants. In the simulation of the measured
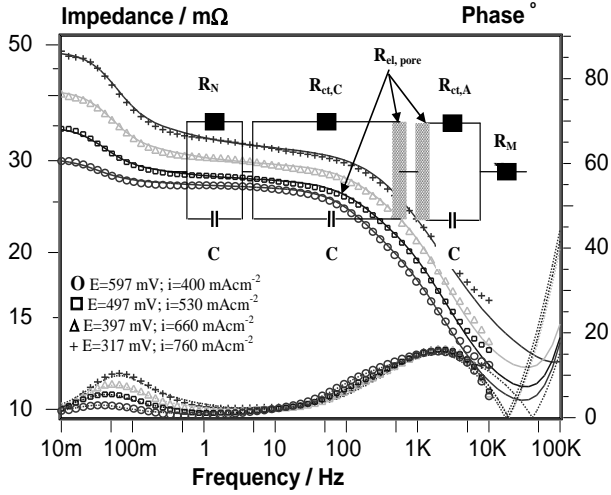
Fig. 4. Bode diagram of EIS measured in the low cell voltage range, at 80°C, at 2 bar absolute, at different cell voltages (currents): (o) 597 V, (□) 497 mV, (Δ) 397 mV and (+) 317 mV with the schematic representation of the used EC for fitting as insert.
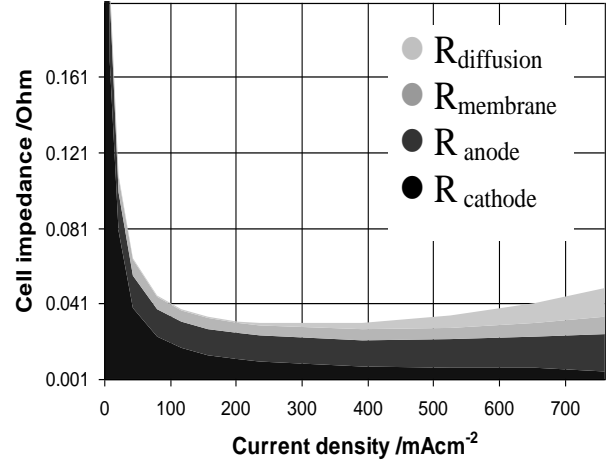

Fig. 5. Current density dependence of different contributions to the overall cell impedance after fitting the measured EIS with the EC from Fig.4.

impedance spectra the ideal capacitance (C) was replaced by CPE (CPE= constant phase element)due to the porous structure of the electrodes. Due to the fact that the electrodes have a porous structure the model of Göhr [1, 3] was used. Taking into account only the electrolyte resistance of the pores filled by electrolyte ($R_{el,pore}$) and the charge transfer resistance (R_{ct}) at the interface porous layer/pore in the porous electrode than we can use a simplified equation (Equ.1) for each polarization resistance (R_p) of the corresponding porous electrode (anode and cathode):

$$R_{p,A} = \frac{\left(R_{el,pore,A} \cdot R_{ct,A}\right)^{\frac{1}{2}}}{\tanh\left\{\left(\frac{R_{el,pore,A}}{R_{ct,A}}\right)^{\frac{1}{2}}\right\}}$$

$$R_{p,C} = \frac{\left(R_{el,pore,C} \cdot R_{ct,C}\right)^{\frac{1}{2}}}{\tanh\left\{\left(\frac{R_{el,pore,C}}{R_{ct,C}}\right)^{\frac{1}{2}}\right\}} \quad (1)$$

The impedance elements $R_{el,pore}$ and R_{ct} from equation (1) are part of the used EC from Fig.4 and the numerical values are obtained after a complex nonlinear last square fit of the measured impedance spectra.

For the oxygen reduction reaction (ORR) at the cathode a parallel R/C term for the charge transfer

through the double layer of the cathode ($R_{ct(C)}$ / $CPE_{dl(C)}$) can be used. A second parallel R/C term for the finite diffusion of water with a Nernst-impedance like behaviour ($R_{(N)}$ / $CPE_{(N)}$) and finally for the simulation of the hydrogen oxidation reaction (HOR) at the anode a third parallel R/C term ($R_{ct(A)}$ / $CPE_{dl(A)}$) can be used. This EC was used to determine the influence of electrolyte (milled Nafion powder) content in the electrode on the electrode (cell) performance [18].

In the impedance spectra (e.g. Fig. 4) we can find the contribution of slow reactions at low frequencies (e.g. diffusion, adsorption, and recrystallization) and the contribution of fast reactions at high frequencies (charge transfer reaction of HOR) [19]. The contribution of electrolyte (membrane) resistance R_M is located at the high frequency end of the impedance spectra, where also some parasitic inductive contribution of connecting wire can be found, especially in the case of very low impedance values.

Using the EC from Fig.4 the numerical values of the resistances, as a function of the applied potential (current density) can be obtained with the complex nonlinear least-square fit program and are represented as a function of the current density in Fig.5. For a more detailed representation of the dependence of the different resistances on current density a linear scale from 0 to 0.2 Ω is used in Fig.5. In the low current density region the cell impedance (resistance) is dominated by the charge transfer resistance of the oxygen reduction reaction. At current densities higher than 236°mAcm^{-2} an additional contribution (diffusion) to the cell impedance is present due to an insufficient
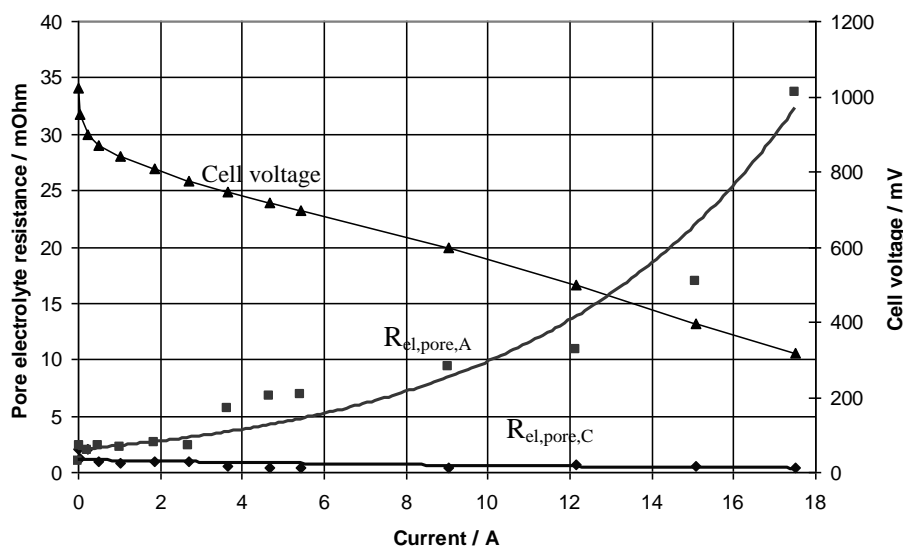
Fig. 6. Current dependence of cell voltage (▲), pore electrolyte resistance of the anode ($R_{el,pore,A}$) (■) and cathode ($R_{el,pore,C}$) (◆).

humidification of the membrane and of the electrolyte component in the anode. The insufficient humidification of the hydrogen feed leads to an increase of the charge transfer resistance of the hydrogen oxidation reaction and also to a strong increase of the pore electrolyte resistance in the anode ($R_{el,pore,A}$ in Fig.6).

The used model (equivalent circuit) for the interpretation of the measured impedance data has to be validated concerning the unambiguous assignment of the impedance elements used in the EC to the electrochemistry of the system by changing some operational conditions like gas composition, partial pressure, concentration, electrode composition, temperature, etc. In the case of PEFC one can also use symmetrical cell configuration or change of the cathode gas supply from pure oxygen to air or changing the anode gas supply from pure hydrogen to CO-containing hydrogen (e.g. H_2 + 100 ppm CO) during constant load of the cell. Another way to validate the used model is to change one of the electrode material or composition, for example using Pt or Pt/Ru anodes for the oxidation of CO-containing hydrogen [20]. During constant load of the cell the anode surface is poisoned and the impedance related to the anode increases due to the decrease of the active anode surface. The impedance of the cathode will remain unaffected from the composition of the anode and in this way one can separate the contribution of the anode and cathode from the cell impedance.

Application of EIS during Oxygen Reduction Reaction in Alkaline Solution

Oxygen reduction electro catalysis is of special importance for fuel cells, metal-air batteries and industrial chlorine-alkali electrolysis as well. Silver is well known as an effective electro catalyst for the reduction of oxygen in alkaline fuel cell cathodes. To enhance his catalytic activity, silver is used in a form with high specific area such as porous electrodes where the silver particles are dispersed in a porous matrix, e.g. PTFE. The porous PTFE-bonded gas-diffusion electrodes can be prepared by a reactive mixing and rolling (RMR) production technique, first described by Winsel [21], and later improved and adapted by other groups [22] or by wet techniques using inks or suspensions. A comprehensive overview on the subject is given in [23]. The electrodes consist of the electrocatalytic active powder (silver, Raney-silver, silver covered with PTFE (Silflon) or silver oxide), the organic binding agent (PTFE), pore forming material (e.g. $NaHCO_3$) and a metal wire gauze to stabilise mechanically the electrode and to collect the current. In gas diffusion electrodes both hydrophobic and hydrophilic pore systems are required. In AFC the hydrophilic system allows the penetration of the electrolyte (alkaline solution) into the electrode and the transport of the ions to or from the reaction zone; in contrast the hydrophobic pore system is required for the transport of the oxygen to the reaction zone. In addition, to give the mechanical stability, the PTFE in the electrodes forms a hydrophobic pore system, whereby a "spider web" of PTFE fibres in and on the electrodes are formed during preparation, as shown

in Fig. 7. Two electrode components Ag and PTFE can clearly be distinguished in Fig. 7. Details of electrode preparation, activation (silver oxide reduction) and experimental set-up are given in [23].
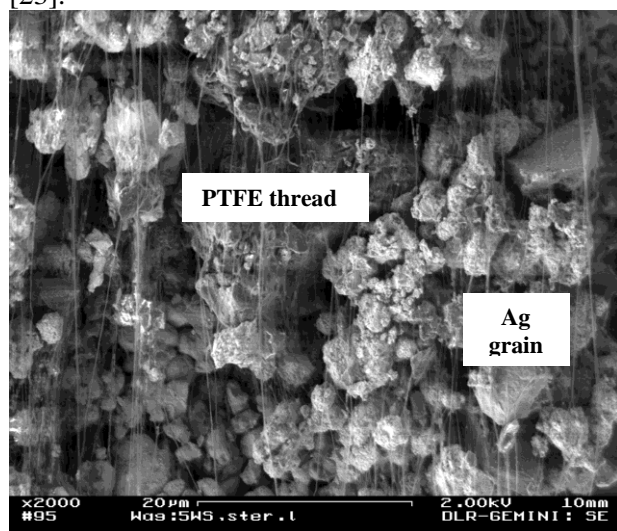

Fig. 7. SEM picture of PTFE bounded silver gas diffusion electrodes (GDE).

Since the electrolyte is a liquid, in contrast to the case of the PEFC the use of a reference electrode (RHE or Hg/HgO) is easily possible and the two electrodes of a fuel cell, anode and cathode can be investigated independent from each other, in half-cell configurations. To indicate the nature of the investigated electrochemical reaction (reduction process) the sign of the current density is negative. Since the kinetics of the oxygen reduction reaction is much slower than the kinetics of the hydrogen oxidation reaction the performance loss of the fuel cell will be determined mainly by the cathode and therefore the oxygen reduction on silver has been investigated by several authors [25–26] with different steady state and potential step techniques on smooth electrodes. The reduction process has been found to follow two reaction pathways [27]: the direct 4e$^-$ path and the 2e$^-$ path (generally referred to as the sequential path) involving the formation of peroxide as an intermediate product.
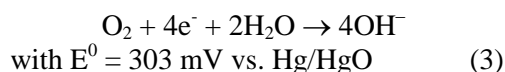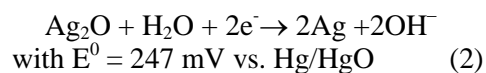
To elucidate the reaction mechanism and to obtain the kinetic parameters for oxygen reduction on PTFE-bonded gas-diffusion silver electrodes in alkaline solution the AC impedance method was applied by several investigators [28–29].

The objective in this second part is to obtain the kinetic parameters for oxygen reduction on PTFE-bonded gas-diffusion silver electrodes in alkaline solution by using cyclic voltammetry (CV) and electrochemical impedance spectroscopy.

The experiments were carried out in a polymethylmetacrylate half-cell with two chambers, a gas chamber and an electrolyte chamber, which are kept tightly together by four screws. The gas chamber has inlet and outlet for the gas flow, while the electrolyte chamber has connections for filling and draining the electrolyte. The working electrode (GDE) is placed between these two chambers and fixed with a sealing rubber. The whole assembly is placed in a thermostatic water bath for carrying out experiments at different temperatures.

Results

The working electrodes were circular PTFE-bonded Gas-Diffusion silver Electrodes (GDE) with an apparent geometric surface area of 1 cm^2. The thickness of the electrode was 0.3 mm. These electrodes were produced by the reactive mixing and rolling (RMR) production technique starting from a powder mixture of silver oxide (Ag$_2$O) and PTFE forming an Ag$_2$O–GDE. This electrode was integrated in a half-cell and reduced in situ electrochemically to silver. The reduction of the silver oxide (2) electrode was performed galvanostatically by applying a current density of -50°mAcm^{-2} (referred to geometric surface area) for 1 hour in 10°N NaOH at 60C. The reduction of silver oxide takes place simultaneously with the oxygen reduction reaction (3):

$$Ag_2O + H_2O + 2e^- \rightarrow 2Ag + 2OH^-$$
$$\text{with } E^0 = 247 \text{ mV vs. Hg/HgO} \qquad (2)$$

$$O_2 + 4e^- + 2H_2O \rightarrow 4OH^-$$
$$\text{with } E^0 = 303 \text{ mV vs. Hg/HgO} \qquad (3)$$

The counter electrode was a Pt-foil. The reference electrode was an Hg/HgO electrode (Ingold Messtechnik, Germany). All potentials are referred to the used Hg/HgO reference electrode, unless otherwise stated. Electrolyte solutions were prepared from analytical grade (Merck) reagents.

2.2.1.1.   Results from CV measurements. All CV measurements were performed in 10 N NaOH solution at 80°C with scan rates of 1 mV/s in the potential range from OCP to -700 mV vs. Hg/HgO (230 mV vs. RHE) and with 50 mV/s in an extended potential range from OCP to an upper potential of 450 mV and in the reverse scan down to -700 mV and back to the starting potential(OCP).
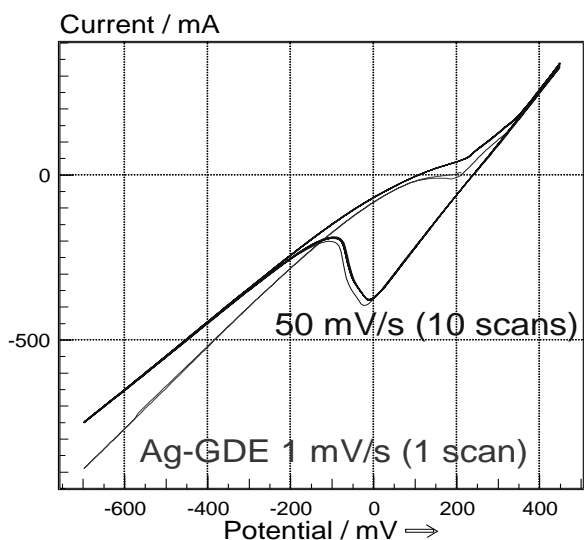
Fig. 8. CV measured during oxygen reduction on Ag-GDE in 10 N NaOH at 80°C with scan rates of 50 mV/s and 1 mV/s.

The Ag_2O reduction peak (Fig.8) appears only in the reverse scan of the spectra recorded up to 450 mV when at potentials higher than OCP the oxidation of silver occurs. This finding suggests that close to OCP both reactions take place: oxidation of silver / reduction of silver oxide and reduction of oxygen.

During CV measurements the electrolyte resistance (R_{el}) was not compensated. Before evaluating the slow CV (1 mV/s) and extracting kinetic relevant parameter first the potentials have to be iR_{el} corrected. The value of R_{el} can be determined from the measured impedance spectra, as shown in the next section. In the CV from Fig.9 uncorrected and iR_{el} corrected potentials referred to the RHE are shown.

Tafel slope and apparent exchange current density can be determined from the Tafel representation of the iR_{el} corrected slow CV from Fig. 9. For more accuracy the current density range was limited in Fig. 10 to the kinetically relevant domain from 0 to -0.1 Acm^{-2}. A Tafel slope of 80 mV/decade and an apparent exchange current density of $4.57\ 10^{-3}$ Acm^{-2} was determined.

Results from impedance measurements.

The electrode impedance was measured with an ac voltage signal in the frequency range from 50 mHz to 100 kHz superimposed on the dc polarisation potential or in the case of galvanostatical control of the half-cell on the dc current. The amplitude of ac signal was kept smaller than 10 mV peak-to-peak in order that the current response remains within a linear range.
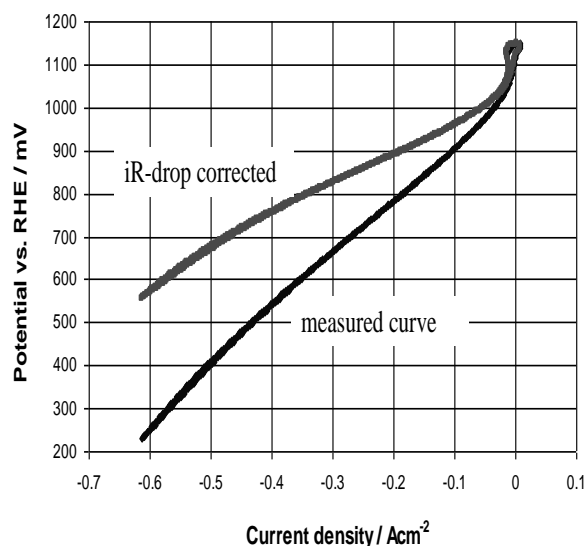

Fig. 9. Uncorrected and iR_{el} corrected data of the CV recorded with 1 mV/s at 80°C during ORR in 10 N NaOH in the potential range from OCP to 230 mV vs. RHE (-700 mV vs. Hg/HgO)
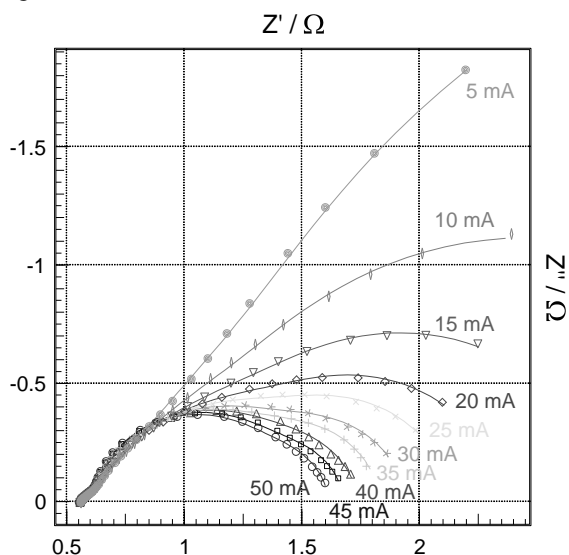
Since the geometric area of the used electrode is 1 cm^2 the measured impedance values correspond to the area-related values.

Impedance spectra have been measured at 80°C, in 10 N NaOH in the low current density range from -5 $mAcm^{-2}$ to -50 $mAcm^{-2}$ (Fig. 11 and Fig. 12).

In order to evaluate the measured impedance spectra and to obtain kinetic data of the oxygen reduction reaction, the reaction steps can be translated into an appropriate equivalent circuit (EC). The evaluation of the measured EIS was performed with a part of EC from Fig. 1 that represents the cathode of the fuel cell, namely the serial combination of Nernst-impedance (diffusion element) and charge transfer resistance connected in parallel with the double layer capacity. These elements are forming the pore's wall surface impedance (Z_q) of the cylindrical-pore model proposed by Göhr. From this model only Z_q and the pore electrolyte (Z_p) impedance (resistance) were considered. The uncompensated electrolyte resistance R_{el} (element 5 from equivalent circuit in Fig.13) is connected in series with the impedance of the porous cathode.
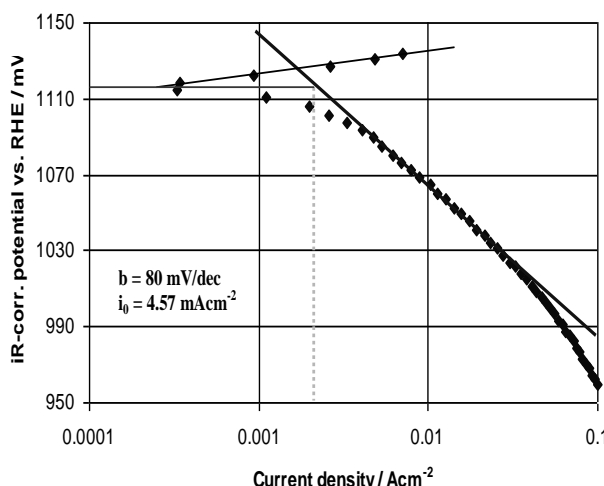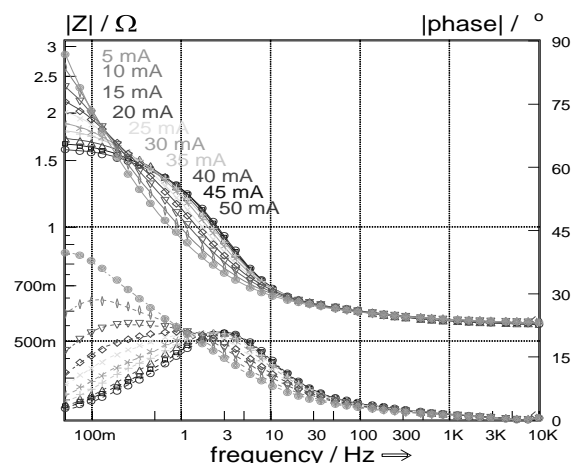
Fig. 10. Tafel-plot of data measured during ORR on Ag-GDE in 10 N NaOH at 80°C.

Fig. 11. Bode representation of impedance spectra measured at different current densities during oxygen reduction reaction on Ag-GDE in 10 N NaOH, 80°C.
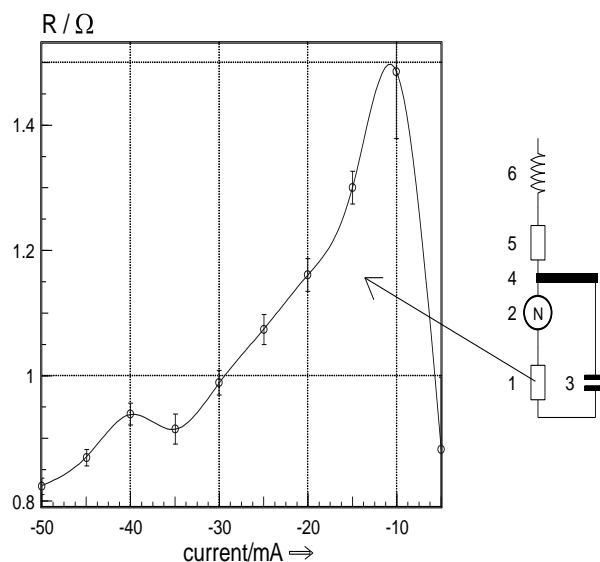

Fig. 12. Nyquist representation of impedance spectra measured in the frequency range from 50 mHz to 10 kHz at different current densities during oxygen reduction reaction on Ag-GDE in 10 N NaOH
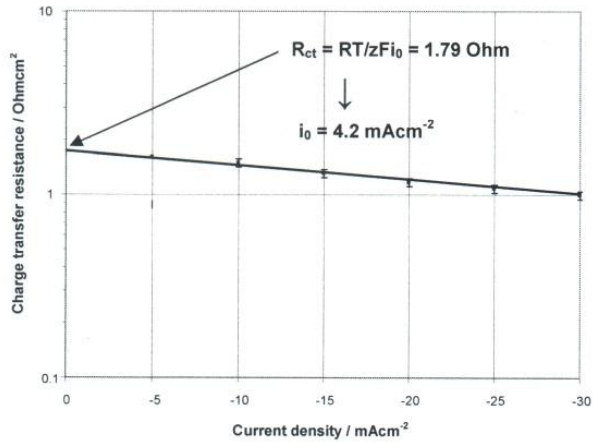

Fig. 13. Current density dependence of the charge transfer resistance (element number 1) during oxygen reduction reaction on Ag-GDE in 10 N NaOH, 80°C.

The current density dependency of the charge transfer resistance R_{ct} and used EC are given in Fig.13. R_{ct} first increase from 0.883 Ωcm^2 at -5 $mAcm^{-2}$ to 1.485 Ωcm^2 at -10 $mAcm^{-2}$ and than decrease to 0.824 Ωcm^2 at -50 $mAcm^{-2}$. This finding suggests that at low current densities close to open cell potential (OCP) two different reactions take place: ORR and silver oxide reduction. At current densities higher than - 10 $mAcm^{-2}$ the oxygen reduction reaction is predominant.

To extract the kinetic data of the OCR the values of R_{ct} were plotted in function of the current density (Fig.14) assuming a Butler-Volmer behaviour. Extrapolating the straight line to zero current one can calculate from the intercept with the y-axis the

value of R_{ct} for the OCR without contributions of the silver oxide reduction reaction. The value calculated for R_{ct} is 1.79 Ωcm^2 and with the formula indicated in the graph one can calculate the apparent exchange current density (i_0) of the oxygen reduction reaction. The calculated value for i_0 is 4.2 $mAcm^{-2}$ and is in good agreement with 4.57 $mAcm^{-2}$ calculated from the CV from Fig. 10.

From the current density dependency of the other impedance elements of the EC, in particular the double layer capacity C (Fig. 15) and electrolyte resistance inside the pore (Fig.16) it is found that with increasing current density the electrochemical active surface and pore electrolyte resistance are increasing. One can
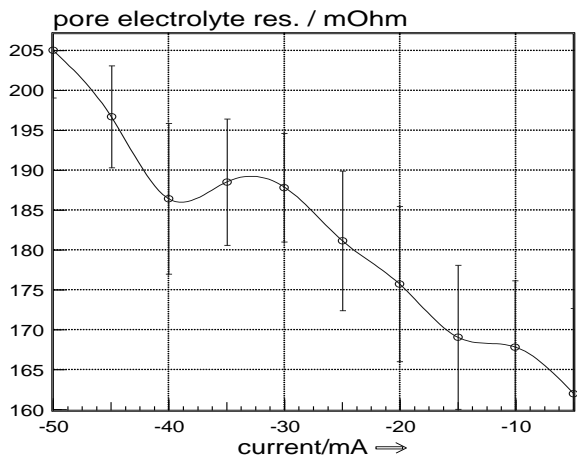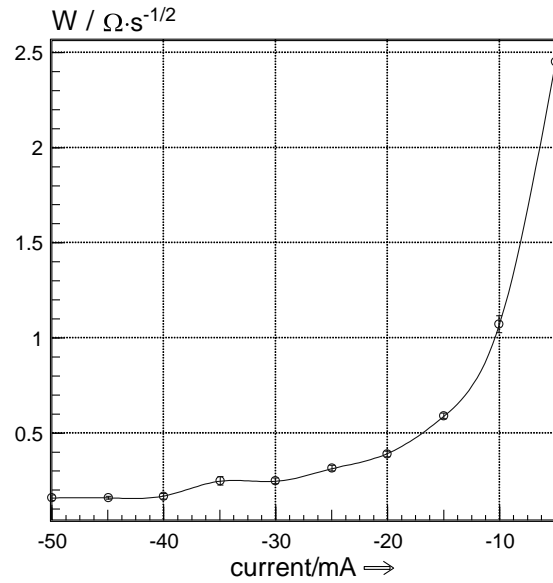
Fig. 14. Low current density dependence of the charge transfer resistance (logarithmical representation) during oxygen reduction reaction on Ag-GDE in 10 N NaOH, 80°C.
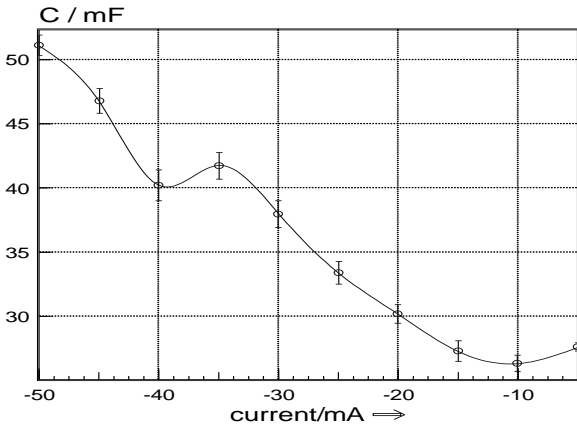
Fig. 15. Current density dependence of the double layer capacity during oxygen reduction reaction on Ag-GDE in 10 N NaOH, 80°C.

Fig. 16. Current density dependence of the pore electrolyte resistance during oxygen reduction reaction on Ag-GDE in 10 N NaOH, 80°C.

Fig. 17. Current density dependency of the Warburg parameter (W) during oxygen reduction reaction on Ag-GDE in 10 N NaOH, 80°C

conclude that in the investigated current density range from OCP to -50 mAcm^{-2} the reaction zone moves with increasing current density within the porous electrode from electrolyte side to gas side. This assumption is confirmed by the current density dependence of the elements of the Nernst-impedance. The Nernst impedance Z_N contains two parameters:the Warburg parameter W with the unit $\Omega s^{-1/2}$ and a diffusion time constant (k_N), determined by the constant of diffusion (D_k) and diffusion layer thickness (d_N). The Nernst impedance is calculated by equation (4):

$$Z_N = \frac{v^2}{z^2} \cdot \frac{R \cdot T}{F^2} \cdot \frac{1}{c_d \cdot \sqrt{D}} \cdot \frac{\tanh\sqrt{\frac{j \cdot \omega \cdot d^2}{D}}}{\sqrt{j \cdot \omega}} \equiv \frac{W}{\sqrt{j \cdot \omega}} \cdot \tanh\sqrt{\frac{j \cdot \omega}{k_N}} \quad (4)$$

The current density dependence of the Warburg parameter (W) is shown in Fig. 17.

The dependence of diffusion layer thickness (d_N) on current density can be evaluated from the value of diffusion time constant k_N (Fig.18) and is calculated by with equation (5). Increasing the current density up to -50 mAcm^{-2} the diffusion layer thickness decreases from 150 μm to 57 μm.

In this work two different formulas for the transfer functions of the diffusion processes were used. In the inset of Fig. 1 a general impedance element Z_{diff} and in the equivalent circuit from Fig.4 a parallel RC-term (R_N and C) is used.

$$d_N = \sqrt{\frac{D}{k_N}} \qquad (5)$$
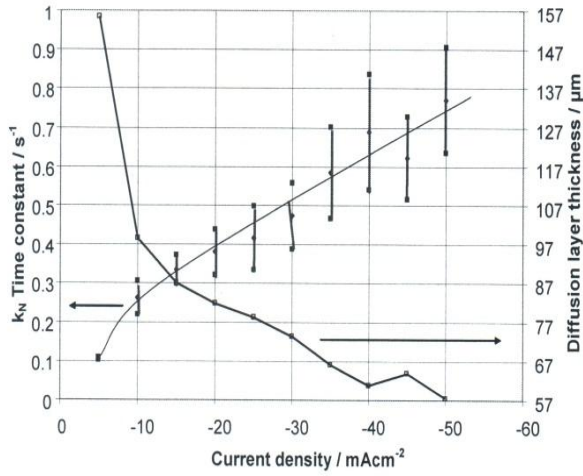
Fig. 18. Current density dependence of the diffusion time constant (2nd parameter of Z_N) and calculated diffusion layer thickness during oxygen reduction reaction on Ag-GDE in 10 N NaOH, 80°C.
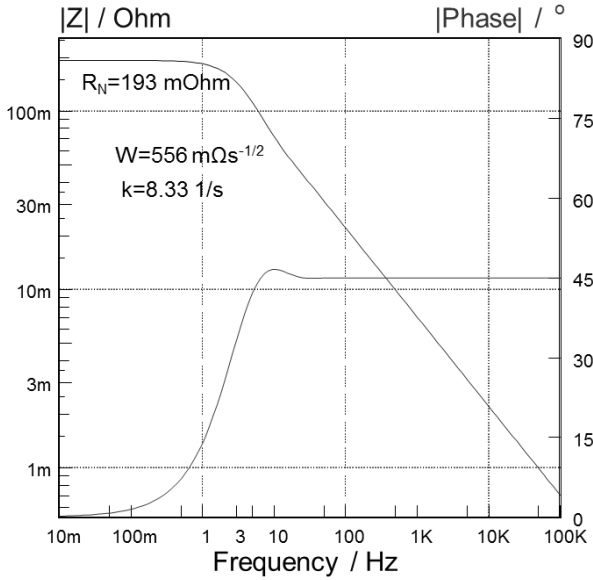
Fig. 19. Bode diagram of simulated impedance spectra of the Nernst impedance Z_N with $W=556$ $m\Omega s^{-1/2}$ and $k_N=8.33$ s^{-1}.

Depending of the boundary condition of the diffusion process we can distinguish between "General Warburg Impedance" element, often called "Nernst diffusion element - Z_N or finite diffusion impedance", with the transfer function given by equation (4), "Special Warburg" diffusion impedance, often called only "Warburg impedance – Z_W or infinite diffusion impedance", with the transfer function given by equation (6).

$$Z_W = \frac{v^2}{z^2} \cdot \frac{R \cdot T}{F^2} \cdot \frac{1}{c_d \cdot \sqrt{D}} \cdot \frac{1}{\sqrt{j \cdot \omega}} \equiv \frac{W}{\sqrt{j \cdot \omega}} \qquad (6)$$

A third kind of diffusion impedance is the finite diffusion impedance Z_S (not used in this work) with the transfer function given by equation (7). Z_S describes a diffusion process where the diffusion length is finite due to a phase boundary assumed in a certain distance from the electrode. This kind of diffusion appears in impedance spectra of batteries e.g. Lithium-ion batteries [30]. The high frequency part of the impedance spectra exhibits the same shape like the Warburg impedance (Special Warburg Impedance) whereas the low frequency part is similar to a capacity.

$$Z_S = \frac{v^2}{z^2} \cdot \frac{R \cdot T}{F^2} \cdot \frac{1}{c_d \cdot \sqrt{D}} \cdot \frac{\coth \sqrt{\frac{j \cdot \omega \cdot d^2}{D}}}{\sqrt{j \cdot \omega}} \equiv \frac{W}{\sqrt{j \cdot \omega}} \cdot \coth \sqrt{\frac{j \cdot \omega}{k_S}} \qquad (7)$$

In the some cases like used in the equivalent circuit in the inset of Fig.4 one can replace Z_N with a parallel combination of R_N and C. This is only true if the argument of the tanh function in equation (3) ω d^2 / D >> 3 so that the equation can be simplified into equation (8):

$$R_N = Z_{N(w=0)} = \frac{v^2}{z^2} \cdot \frac{R \cdot T}{F^2} \cdot \frac{1}{c_d \cdot \sqrt{D}} \cdot \frac{1}{\sqrt{j \cdot \omega}} \equiv \frac{W}{\sqrt{k_N}} . \qquad (8)$$

The validation of equation 8 is demonstrated in Fig. 19 by using one value (W=556 $m\Omega s^{-1/2}$ and $k_N=8.33$ s^{-1}) of the Nernst impedance from Fig. 13. The low frequency limit of Z_N is identical with R_N calculated with equation (8).

3. CONCLUSION

The evaluation of EIS using the porous electrode model proposed by Göhr is very helpful to understand some important features of fuel cell electrodes and operating conditions. In the case of PEFC it could be shown that insufficient humidification of the anode leads to an increase of performance loss not only due to the well-known increase of the membrane resistance (R_M) but also due to an increase of pore electrolyte resistance inside the anode affecting the electrode composition, in particular the content of solid electrolyte in the anode [18]. An increase of pore electrolyte resistance in the anode ($R_{el,pore,A}$ in Fig.6) increases the potential drop in the anode and contribute to an increase of performance loss of the anode and fuel cell respectively.

In the case of silver gas diffusion electrodes used for the oxygen reduction in alkaline solution it could be shown the movement of reaction zone

inside the GDE and change of diffusion layer thickness with current density in the current density range from 0 to -50 mAcm^{-2} .

REFERENCES:

1. N. Wagner, "Electrochemical power sources – Fuel cells" in *Impedance Spectroscopy: Theory, Experiment, and Applications*, 2nd Edition, Edited by Evgenij Barsoukov and J. Ross Macdonald, John Wiley&Sons, Inc., ISBN: 0-471-64749-7, pp. 497-537, (2005).

2. P. Spinelli, C. Francia, E.P. Ambrosio, M. Lucariello, *J. Power Sources* **178,** 517, (2008).

3. H. Göhr, *Electrochemical Applications* **1**, 2, (1997) (http://www.zahner.de)

4. D.P. Davies, P.L. cAdcock, M. Turpin, S.J. Rowen, *J. Power Sources* **86,** 237, (2000).

5. B. Mattsson, H. Ericson, L.M. Torell, F. Sundfolm, *Electrochim. Acta* **45,** 1405, (2000).

6. A.S. Aricò, A. Stassi, E. Modica, R. Ornelas, I. Gatto, E. Passalacqua, V, Antonucci, *J.Power Sources* **178,** 525, (2008).

7. M. Schulze, M. Lorenz, N. Wagner, E. Gülzow, *FreseniusJ. Anal. Chem.* **365,** 106, (1999).

8. F. N. Büchi, B. Gupta, O. Haas, G.G. Scherer, *Electrochim. Acta* **40,** 345, (1995).

9. E. Gülzow, A. Helmbold, T. Kaz, R. Reißner, M. Schulze, N. Wagner, G. Steinhilber, *J. Power Sources* **86,** 352, (2000).

10. M. Schulze, N. Wagner, T. Kaz, K.A. Friedrich, *Electrochim. Acta* **52,** 2328, (2007).

11. E. Gülzow, M. Schulze, G. Steinhilber, *J. Power Sources* **106,** 126, (2002).

12. Y. Kiros, S. Schwartz, *J. Power Sources* **87,** 101, (2000).

13. N. Wagner, M. Schulze, E. Gülzow, *J. Power Sources* **127,** 264, (2004).

14. F. Richter, C.-A. Schiller, N. Wagner, Current Interrupt Technique-Measuring low impedances at high frequencies, in „Electrochemical Applications, 1/2002", p.1-6, Ed. Zahner-elektrik, Kronach, 2002

15. N. Wagner, T. Kaz, K.A. Friedrich, *Electrochim. Acta* **53,** 7475, (2008).

16. N. Wagner, *J. Appl. Electrochem.* **32**, 859, (2002).

17. X. Yuan, H. Wang, J.C. Sun, J. Zhang, *Int. J. Hydrogen Energy* **32,** 4365, (2007).

18. N. Wagner, T. Kaz, K. A. Friedrich, *Electrochim. Acta* **53,** 7475, (2008).

19. N. Wagner, K.A. Friedrich, Dynamic Operational Conditions. In J. Garche, C. Deyer, P. Moseley, Z. Ogumi, D. Rand and B. Scrosati (Eds.). Encyclopedia of Electrochemical Power Sources, Vol.2, ISBN-978-0-444-52093-7, Amsterdam, Elsevier 2009, pp. 912-930.

20. N. Wagner, M. Schulze, *Electrochim. Acta* **48,** 3899, (2003).

21. A. Winsel, German Patent, DE 3342969, 1985.

22. N. Wagner, German Patent, DE 199 40 015, 2004.

23. I. Moussallem, J. Jörissen, U. Kunz, S. Pinnow, T. Turek, *J. Appl. Electro*chem. **38,** 1177, (2008).

24. E. Gülzow, N. Wagner and M. Schulze, *Fuel Cells – From Fundamentals to Systems* **3** 67, (2003).

25. P. Fischer, J. Heitbaum, *J. Electroanal. Chem.* **112,** 21, (1980).

26. B.D. Cahan, J.B. Ockerman, R.F. Amlie, P.Rüetschi, *J. Electrochem. Soc*. **107,** 725, (1960).

27. J.P. Hoare, The Electrochemistry of Oxygen, Interscience, New York, 1968

28. K. Mund, *Siemens Forsch.- und Entwickl.- Ber*. **4,** 68, (1975).

29. R. Holze, W. Vielstich, *J. Electrochem. Soc*. **131,** 2298, (1984).

30. M. Chamas, P-E. Lippens, J-C. Jumas, J. Hassoun, S. Panero, B. Scrosati, *Electrochim. Acta* **56,** 6732, (2011).

ПРИЛОЖЕНИЕ НА ЕЛЕКТРОХИМИЧНА ИМПЕДАНСНА СПЕКТРОСКОПИЯ ЗА ОХАРАКТЕРИЗИРАНЕ НА ГОРИВНИ ЕЛЕМЕНТИ: ГОРИВЕН ЕЛЕМЕНТ С ПОЛИМЕРЕН ЕЛЕКТРОЛИТ И РЕАКЦИЯ НА РЕДУКЦИЯ НА КИСЛОРОДА В АЛКАЛЕН РАЗТВОР

Н. Вагнер

Германски аерокосмически център, Институт по техническа термодинамика, Пфафенвалдринг 38-40, D-70569, Щутгарт, Германия

(Резюме)

Един от най-разпространените методи за охарактеризиране електрохимичните отнасяния на горивни елементи е регистрирането на волтамперните U(i) криви. Разделянето на електрохимичния от омовия принос към волтамперните характеристики изисква допълнителни експериментални техники като електрохимична импедансна спектроскопия (IES) и токово въздействие (CI). Прилагането на EIS е *in-situ* подход за определяне на параметри, които се оказват незаменими за характеризирането и разработването на всички видове електроди и агрегати електрод-електролит за горивни елементи [1]. Освен IES, за напасването на експерименталните U(i) криви могат да се използват полуемпирични подходи, основани на опростени математически модели [2].

Импедансът на горивния елемент може да бъде разделен на електроден импеданс и съпротивление на електролита чрез промяна на работните условия на горивния елемент и симулиране на измерената EIS с подходяща еквивалентна схема. Като се интегрират отделните елементи на импеданса в токовата област, може да се пресметнат отделните свръхнапрежения в горивния елемент и падовете на напрежение да се припишат на различните процеси. При триелектродна конфигурация на клетката със сравнителен електрод, съответното свръхнапрежение може да бъде определено директно. Моделът на порист електрод на Göhr [3] е използван за оценка на измерените импедансни спектри. Моделът на порист електрод включва различни приноси към импеданса като импедансите на граничните повърхности порист слой/пора, порист слой/електролит и порист слой/обемен материал, импедансът на самия порист слой и импедансът на запълнената с електролит пора